Electrical and optical evaluation of n-type doping in $In_xGa_{(1-x)}P$ nanowires

Zeng, Xulu; Mourao, Renato T.; Otnes, Gaute; Hultin, Olof; Dagyte, Vilgaile; Heurlin, Magnus; Borgström, Magnus T.

Published in:
Nanotechnology

DOI:
10.1088/1361-6528/aabaa5

2018

Document Version:
Peer reviewed version (aka post-print)

Electrical and optical evaluation of *n*-type doping in $In_xGa_{(1-x)}P$ nanowires

Xulu Zeng[1,*], Renato T. Mourão[2,*], Gaute Otnes[1,*], Olof Hultin[1], Vilgailė Dagytė[1], Magnus Heurlin[1,3], Magnus T.Borgström[1]

*These authors contributed equally to this work

[1] Solid State Physics, NanoLund, Lund University, PO Box 118 Lund, Sweden

[2] Instituto de Física, Universidade Federal do Rio de Janeiro, Caixa Postal 68528, 21941-972 Rio de Janeiro, Brazil

[3] Present address: Sol Voltaics AB, Ideon Science Park, Scheelevägen 17, SE-22370 Lund, Sweden

Abstract

To harvest the benefits of III-V nanowires in optoelectronic devices, the development of ternary materials with controlled doping is needed. In this work, we performed a systematic study of *n*-type dopant incorporation in dense $In_xGa_{(1-x)}P$ nanowire arrays using tetraethyl tin (TESn) and hydrogen sulfide (H_2S) as dopant precursors. The morphology, crystal structure and material composition of the nanowires were characterized by use of scanning electron microscopy, transmission electron microscopy and energy dispersive x-ray analysis. To investigate the electrical properties, the nanowires were broken off from the substrate and mechanically transferred to thermally oxidized silicon substrates, after which electron beam lithography and metal evaporation were used to define electrical contacts to selected nanowires. Electrical characterization, including four-probe resistivity and Hall effect, as well as back-gated field effect measurements, is combined with photoluminescence spectroscopy to achieve a comprehensive evaluation of the carrier concentration in the doped nanowires. We measure a carrier concentration

of ~1 × 10^{16} cm^{-3} in nominally intrinsic nanowires, and the maximum doping level achieved by use of TESn and H_2S as dopant precursors using our parameters is measured to be ~2 × 10^{18} cm^{-3}, and ~1 × 10^{19} cm^{-3}, respectively (by Hall effect measurements). Hence, both TESn and H_2S are suitable precursors for a wide range of *n*-doping levels in $In_xGa_{(1-x)}P$ nanowires needed for optoelectronic devices, grown via the vapor–liquid–solid mode.

Introduction

Nanowires with their unique properties and great potential in next generation semiconductor devices are under intensive investigation. For instance, in the field of photovoltaics, a substrate surface covered with evenly-spaced particle-assisted-grown nanowires (i.e. a nanowire array) has achieved a power conversion efficiency of 15.3% by covering only 13% of the substrate surface [1]. Also, the small radial dimension of nanowires allows a variety of material combinations to be grown, since the strain can be accommodated via radial expansion and contraction [2]. Even material combinations with very high lattice mismatch and therefore unrealistic in planar growth, like InSb/GaAs, have been reported in nanowires [3]. In this sense, nanowire arrays introduce a highly interesting geometry for the production of multi-junction (tandem) solar cells. Such structures are comprised of a combination of several *p*-*n* (or *p*-*i*-*n*) junctions with different band gaps to efficiently match the solar spectrum, where the increased freedom of material combinations in the nanowire geometry facilitates synthesis. To make full use of this potential, the growth of ternary III-V nanowires with controlled doping must be developed.

The control of dopant incorporation is vital for the electrical and optical performance of any semiconductor device. Significant knowledge has been accumulated on doping of nanowires [4], with quantitative data obtained by a wide range of methods such as field-effect transistor [5], Hall

effect [6, 7], atom probe tomography [8], photoluminescence (PL) [9], Raman [10], and capacitance–voltage [11] measurements. However, most studies have been carried out on various elemental or binary materials [12], and very little has been done on doping in ternary nanowires, especially in terms of systematic quantitative studies. We are interested, at first, to achieve controlled n- and p-type doping in nanowires of the ternary alloy InxGa(1−x)P with a band gap of 1.7 eV to be used as a top cell in a proposed InxGa(1−x)P/InP tandem junction solar cell [13]. A detailed study on p-type doping in this material has been reported elsewhere [14]. In the current paper, we report on the growth of InxGa(1−x)P nanowire arrays in the right composition range and evaluation of two different n-type dopant precursors by electrical and optical characterization.

Experimental

The $In_xGa_{(1-x)}P$ nanowires were grown on InP:Zn (111)B substrates. Full 2 inch wafers were patterned by an array of Au seed particles by nanoimprint lithography and metal evaporation as described in [15]. The resulting hexagonal pattern had a pitch of 0.50 µm, with gold particles in the form of discs with 0.19 µm in diameter and 0.07 µm in height. The wafer was split into smaller substrate pieces which were loaded into an Aixtron 200/4 metal organic vapor phase epitaxy (MOVPE) reactor, operating at 100 mbar in a total flow of 13 l/min. Using parameters as described in [15], a pre-anneal nucleation step was used to reduce particle displacement, followed by an annealing step at 550 °C. Then, the reactor temperature was set to 440 °C. A series of $In_xGa_{(1-x)}P$ nanowire samples were grown, based on the structure sketched in figure 1a. Here, 300 nm long contact segments were grown at each end of the nanowire, with constant growth parameters between all samples. In between the contact segments, a 1.6-1.7 µm long segment was grown where the dopant values were varied between samples. Before growth of the first contact segment, the growth was

initiated with an approximately 0.15 µm long InP stub with trimethylindium (TMIn), and phosphine (PH_3), at molar fractions of $\chi_{TMIn}= 8.9 \times 10^{-5}$, $\chi_{PH3} = 6.9 \times 10^{-3}$ (Fig. 1a) [14]. Thereafter, both contact segments and the middle segment were grown using the precursors of TMIn, trimethylgallium (TMGa) and PH_3, at molar fractions of $\chi_{TMIn}= 2.7 \times 10^{-5}$, $\chi_{TMGa}= 1.36 \times 10^{-3}$, and $\chi_{PH3}= 5.4 \times 10^{-3}$. During the nanowire growth, hydrogen chloride (HCl) was supplied in situ with a molar fraction of $\chi_{HCl}= 5.4 \times 10^{-5}$ to suppress radial growth [16]. In terms of doping, the contact segments were grown with the same TESn flow for all samples, $\chi_{TESn} = 5.5 \times 10^{-5}$, to provide similar Ohmic contacts for all the nanowires studied [17]. In the middle segment on the other hand, the molar fraction was different between samples, with the dopant precursor being either TESn or H_2S. In the sample ensemble, χ_{TESn} was varied from 3×10^{-6} to 5.5×10^{-5}, and χ_{H2S} was varied from 1×10^{-7} to 3.12×10^{-5}. Additionally, one sample was grown as a reference with the middle segment nominally intrinsic ($\chi_{TESn,H2S} = 0$). The nanowire length was continuously monitored in situ by an EpiR DA UV optical reflectance setup from LayTec AG [14,18] and the growth time was adjusted to achieve the appropriate segment lengths. After nanowire growth, the reactor was cooled down to room temperature in a PH_3 ambient. A scanning electron microscope (SEM) image of a typical nanowire sample is depicted in figure 1b.

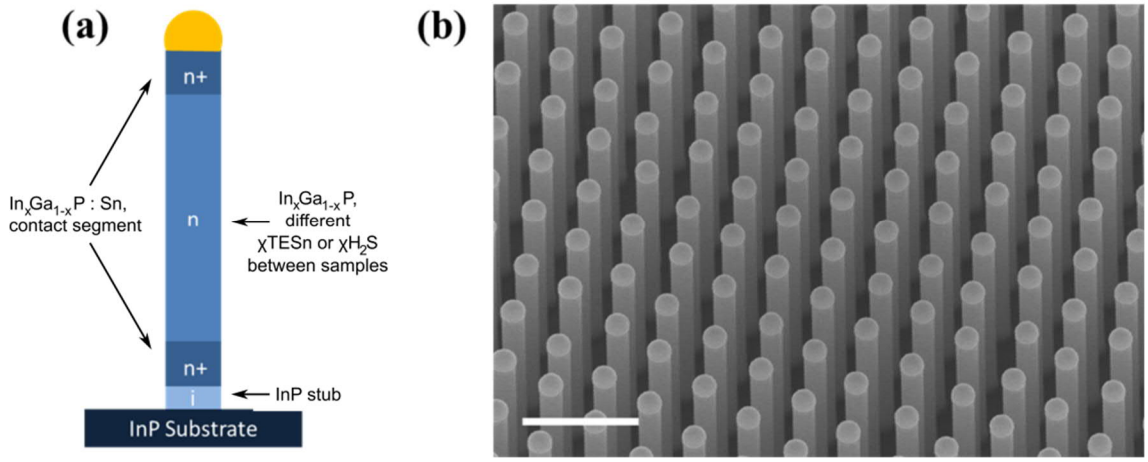

Figure 1. (a) Schematic of the nanowire structure. (b) Scanning electron microscope image of as-grown $In_xGa_{(1-x)}P$ nanowire arrays, taken at 30° tilt. The scale bar is 1 µm.

The crystal structure of the nanowires was inspected by a JEOL 3000F 300 kV transmission electron microscope (TEM) equipped with energy dispersive x-ray analysis (EDX) by which the nanowire composition along its axis was measured. Three different samples, each with a unique dopant flow, i.e. nominally intrinsic, the highest TESn flow and the highest H_2S flow were chosen. Three nanowires for each chosen sample were measured.

For electrical characterization, the nanowires were transferred from the growth substrate to a doped Si measurement substrate covered by 100 nm SiO_2 and 10 nm HfO_2. The measurement substrates had predefined bond pads and markers for contact alignment. Contacts were defined to the nanowires by electron beam lithography (EBL). The devices were etched for 15 s in Buffered Oxide Etch (H_2O:HF = 10:1) to remove native oxides right before thermal evaporation of 10 nm Ti and 150 nm Au. Lift-off was done in acetone. A typical processed nanowire is shown in figure 2. The contacts were labeled as “A” and “B” at the two ends of the nanowire, and the three pairs, labeled as “C1”, “C2”, “D1”, “D2”, “E1” and “E2”, are perpendicular to the nanowire axis. These contacts were designed to allow for four-probe resistivity measurements and Hall-effect measurements with spatial resolution of the carrier concentration along the nanowire growth direction [6,19]. The four-probe resistivity measurements were conducted at room temperature by use of a Cascade 11000B probe station and a Keithley 4200SCS. The Hall-effect measurements were carried out in room temperature using a custom made system [20].

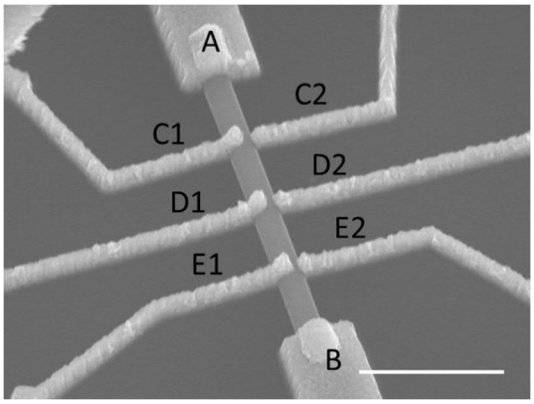

Figure 2. Scanning electron microscope image of a typical device after processing, taken at 30° tilt with respect to the normal of the plane, showing contact design for electrical measurements. The contacts labelled as pairs "C","D" and "E" are at 30%, 50% and 70% of the nanowire length. The scale bar is 1 µm.

For four-probe resistivity measurements, voltage sweep was done between contacts A and B (see figure 2), and the resulting current was measured. The voltage at the different positions C, D, and E along the device was also measured, and the electrical resistance of each segment was calculated by dividing the voltage ΔV_c between each contact pair C1-D1, D1-E1 and C1-E1 (same for side 2) by the current. We refer to the measurements at pairs C-D, C-E and D-E as "base", "center" and "top", respectively. In the Hall-effect measurement setup, a current of 100 µA was applied between contacts A and B, and a magnetic field ranging from -2.0 to 2.0 T was applied perpendicular to the substrate plane and the current direction. The Hall voltage was then measured between each pairs C1-C2, D1-D2 and E1-E2 (referred to as "base", "center" and "top", respectively). A plot of example Hall measurements is included in the Supporting Information. In order to extract the carrier concentration from the measurements, a finite-element-method model implemented in COMSOL Multiphysics was used to solve the current continuity equation and simulate the carrier concentration corresponding to the measured Hall voltage in each nanowire [6]. The input parameters were the nanowire length, diameter and contact positions.

Photoluminescence (PL) measurements were performed on single nanowires, which were mechanically transferred to silicon substrates. The samples were placed in a continuous-flow liquid-helium-cooled cold finger cryostat for measurement at around 4K. The sample was excited by a frequency-doubled YAG laser, and the photoluminescence from the sample was then collected by a microscope objective, dispersed by a monochromator and finally analyzed by a CCD camera. By comparing the high energy tail of a PL spectrum, which contains information about Fermi level, with the high energy tail of the conduction band density of occupied states, the Fermi level and Fermi temperature can be extracted. The extracted values are then used to solve a Fermi-Dirac integral numerically, resulting in a carrier concentration value [21].

Results and discussion

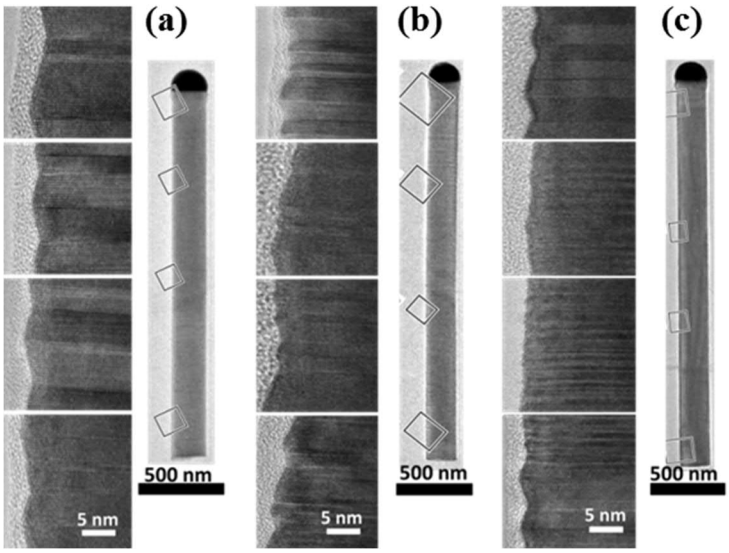

Figure 3. HRTEM images for three different molar fractions in the middle segments: (a) nominally intrinsic $\chi_{TESn,H2S} = 0$, (b) highest TESn flow, $\chi_{TESn} = 5.5\times 10^{-5}$, and (c) highest H_2S flow, $\chi_{H2S} = 3.12\times 10^{-5}$.

As depicted in figure 3, the nominally intrinsic $In_xGa_{(1-x)}P$ nanowires show dislocation-free Zincblende crystal structure with twin planes, and the most highly Sn doped nanowires contain

similar crystal structure. Thus, we did not identify any effect of using TESn as a dopant precursor on the crystal structure, similar to results on Sn doped InP nanowires [22]. In contrast, the middle segments of the most highly S doped nanowires show a mixed crystal structure, consistent with observations in InP nanowires where H_2S induces more Wurtzite structure [23,24].

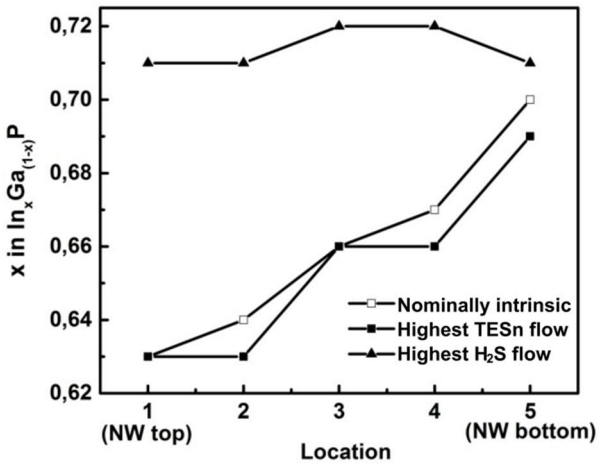

Figure 4. Energy dispersive x-ray (EDX) point scans along the $In_xGa_{(1-x)}P$ nanowires of three representative samples: nominally intrinsic, the highest TESn flow and highest H_2S flow. The five points are along the middle segment of the nanowire, where 1 represents the point closest to the nanowire top, and 5 represents the point closest to the nanowire bottom.

The incorporation of S into the seed particle changes the surface energy of the particle [24]. It is believed that S is usually a surface passivator of liquid metal particles and reduces the liquid–vapor surface energy γ_{LV}. S also increased the wetting of In which means the liquid–solid energy γ_{LS} is also lowered. When both γ_{LV} and γ_{LS} are decreased, the solid–vapor interface would play a more important role at the triple phase boundary where the formation of Wurtzite structure can happen [23].

The averages of the EDX data taken (plotted in figure 4) show that the overall compositions for all three samples are fairly similar, in the range of $0.63 < x < 0.71$. This agrees with ensemble measurements by XRD (not shown), which indicated no clear trends in composition as a function

of doping. However, for the nominally intrinsic and Sn doped samples, the EDX data indicate a relatively large composition gradient along the nanowire axis (about 6% - 7% points), with more Ga rich composition at the top of the nanowires. This is due to a lowered incorporation of surface-migration-limited In along the length of the nanowire [14]. In contrast, the S doped nanowires are more homogenous in material composition (For the highest χ_{H2S}, the composition gradient is less than 1% point). Relating to this, we observe an increasing nanowire growth rate with increased χ_{H2S} (see Supporting information figure S1 for a plot of nanowire length vs. growth time for different χ_{H2S}). The increased growth rate can be attributed to S passivation of the nanowire side walls and substrate surface [24], leading to an increase in the adatom surface migration length, in accordance with our previous study on S doped InP nanowires grown from the same seed particle pattern [20]. This can also explain the improvement in axial material composition homogeneity.

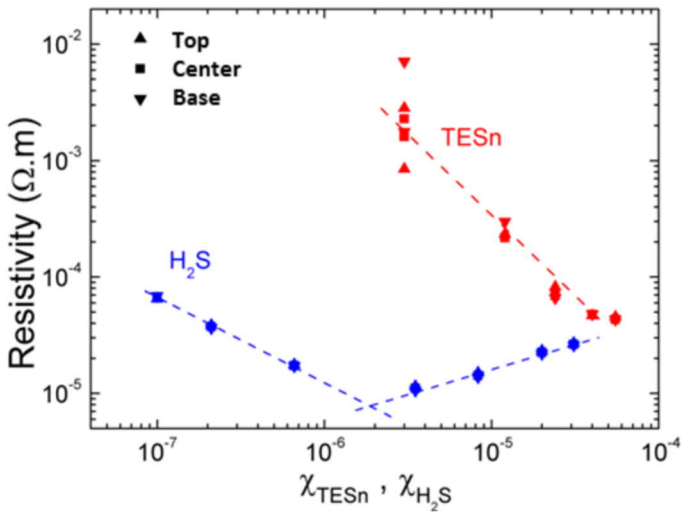

Figure 5. Spatially resolved four-probe resistivity along the length of Sn and S doped $In_xGa_{(1-x)}P$ nanowires. The dashed lines are guides for the eye.

The spatially resolved resistivity extracted from four probe measurements is shown in figure 3 as a function of χ_{TESn} and χ_{H2S}. The data from Sn and S doped samples are indicated in red and blue, respectively. In the Sn doped nanowires, the resistivity decreases as the dopant flow is

increased. In contrast, the S doped nanowires show a change in trend when increasing the dopant flows beyond a certain value, as indicated in figure 5; the resistivity decreases for $\chi_{H2S} < 7\times 10^{-7}$, then increases for $\chi_{H2S} > 3.5\times 10^{-6}$.

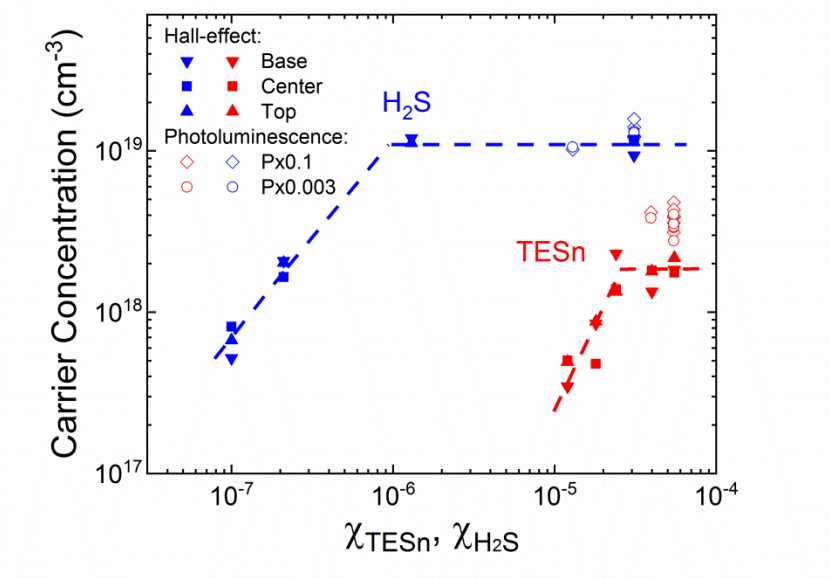

Figure 6. Dependence of carrier concentration measured by Hall-effect measurements on dopant molar fractions. The dashed lines are guide for the eyes. Also included are carrier concentrations extracted from Fermi tail fitting of the PL spectra for the two highest dopant molar fractions of H_2S and TESn. Results are shown from measurements at two different excitation powers to indicate that there is no strong state filling effect.

Extracted carrier concentration values from Hall-effect measurements for different samples are shown in figure 6. For the S doped nanowires, the measured carrier concentration initially increases with dopant molar fraction, until the carrier concentration saturates at around 1×10^{19} cm^{-3} for $\chi_{H2S} \geq 1.3 \times 10^{-6}$. The onset of saturation happens at dopant flows close to the minimum resistivity in figure 5, indicating that the increase in resistivity values seen for higher dopant flows (figure 5) is due to a decrease in electron mobility, possibly due to increased scattering from defects such as S clustering, S-complex formation and donors. For Sn doped nanowires, although not as clear as for samples doped with S, the data suggest carrier concentration saturation at around 2 ×

10^{18} cm^{-3}, after an initial increase in carrier concentration upon increased dopant molar fraction. The Vapor-Liquid-Solid mechanism for nanowire growth is very different from that of planar growth. S has a low solubility in the Au particle and is mainly incorporated via the transportation from the nanowire sidewalls, i.e. a vapor-solid route [25]. By contrast, Sn has a high solubility in the Au particle and the main route for its incorporation is via VLS mechanism. The different incorporation routes can give different maximum doping level. Additionally, S has shown a much larger segregation coefficient (0.5) compared to that of Sn (0.02) in thin film InP growth [26], which can increase the saturation doping level of S compared to Sn.

It has been observed that carrier concentration levels might vary axially in nanowires, even when the dopant flow is kept constant during growth [27]. For instance, in InP nanowires with a similar design as the $In_xGa_{(1-x)}P$ nanowires studied here, we have previously measured axial variation in carrier concentration levels of more than one order of magnitude [19]. In comparison, the spatially resolved Hall effect measurements (figure 6) indicate an axial variation in carrier concentration levels in our $In_xGa_{(1-x)}P$ nanowires of less than a factor of two for all samples, with most samples showing variation below 50%. The small spatial variation in measured resistivity values (figure 5) further supports this picture. For the nominally intrinsic $In_xGa_{(1-x)}P$ nanowire sample ($\chi_{TESn,H2S} = 0$), we were not able to perform Hall-effect measurements because the Hall-contact properties were too poor. Instead, we performed four-probe resistivity and nanowire FET measurements and obtained a background doping of 1.1×10^{16} cm^{-3}. This is similar to the background doping of 1.8×10^{16} cm^{-3} measured by the same method on the nominally intrinsic InP nanowires grown from the same seed particle pattern [20].

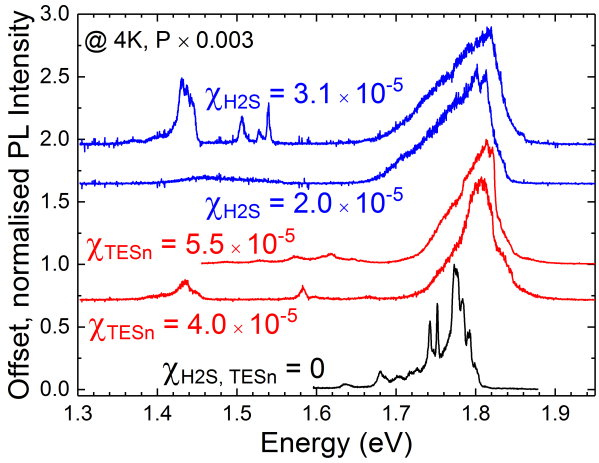

Figure 7: PL at 4K at low excitation power, comparing intrinsic NW sample to Sn and S doped samples. The data shown are for one single wire for each molar fraction value.

PL measurement is a rapid method for measuring carrier concentration, which requires no prior processing and provides good agreement with Hall-effect measurements [21]. By fitting the high energy tail of the spectrum (example spectra shown in figure 7), a carrier concentration can be extracted. The carrier concentrations extracted in this way are plotted in figure 6 together with the Hall data for the two highest dopant flows of TESn and H_2S. The carrier concentration for the highest S doped sample was estimated from PL to be $1.3 \pm 0.1 \times 10^{19}$ cm^{-3}, agreeing well with the Hall-effect measurements (doping saturation at ~1×10^{19} cm^{-3}). Taking Hall-effect and PL measurements together, it is clear that the highest S doped $In_xGa_{(1-x)}P$ nanowires have reached degenerate doping. For the highest Sn doped sample, the carrier concentration obtained from PL measurements was estimated to $3.7 \pm 0.5 \times 10^{18}$ cm^{-3}, roughly a factor of 2 higher than the Hall-effect measurements result (1.9×10^{18} cm^{-3}). By interpolation of the parameters of binary components, degenerate *n*-doping levels for $In_xGa_{(1-x)}P$ can be estimated to $6.1 \times 10^{17} – 6.5 \times 10^{17}$ cm^{-3} [28] (Interpolation method is described in the supporting information). Taken together with an observed blue shift of the high energy side of the spectra in the highest Sn doped samples (figure

7), our data indicate that close to degenerate doping levels in the $In_xGa_{(1-x)}P$ nanowires are possible also when using Sn as a dopant.

Conclusions

We have demonstrated in situ *n*-type doping of $In_xGa_{(1-x)}P$ nanowires by using TESn and H_2S as dopant precursors and evaluated the carrier concentration by combining electrical and optical measurements. Using both TESn and H_2S, we observe an increase in carrier concentration levels for increasing dopant molar fraction, until the carrier concentration saturates. This saturation occurs at lower dopant molar fraction and at higher carrier concentration levels for H_2S than for TESn. We measure a carrier concentration of 1×10^{16} cm^{-3} in nominally intrinsic nanowires, and the maximum doping level achieved by use of TESn and H_2S as dopant precursors is measured to be ~2×10^{18} cm^{-3}, and ~1×10^{19} cm^{-3}, respectively (by Hall effect measurements) under our parameters. The carrier concentration levels extracted by use of Hall-effect and PL measurements agree well.

Our data indicate that both TESn and H_2S can be used as precursor for high control over n type doping in $In_xGa_{(1-x)}P$ nanowires intended for solar cells and other optoelectronic devices.

Acknowledgement

This study was performed within NanoLund and Myfab and was supported by the Swedish Research Council (Vetenskapsrådet), the Swedish Foundation for Strategic Research (SSF), the Knut and Alice Wallenberg Foundation, the Swedish Energy Agency and CAPES – Coordination for the Improvement of Higher Education Personnel (Brazil). This project has received funding

from the European Union's Horizon 2020 research and innovation programme under grant agreement No 641023 (Nano-Tandem) and the European Union's FP7 programme under grant agreement No 608153 (PhD4Energy). This publication reflects only the author's views and the funding agency is not responsible for any use that may be made of the information it contains.

References

[1] Åberg I, Vescovi G, Asoli D, Naseem U, Gilboy J P, Sundvall C, Dahlgren A, Svensson K E, Anttu N, Bjork M T and Samuelson L 2016 A GaAs Nanowire Array Solar Cell With 15.3% Efficiency at 1 Sun *IEEE J. Photovoltaics* **6** 185–90

[2] Glas F 2006 Critical dimensions for the plastic relaxation of strained axial heterostructures in free-standing nanowires *Phys. Rev. B* **74** 121302

[3] Caroff P, Dick K A, Johansson J, Messing M E, Deppert K and Samuelson L 2009 Controlled polytypic and twin-plane superlattices in III-V nanowires. *Nat. Nanotechnol.* **4** 50–5

[4] Dayeh S. A., Chen R., Ro Y. G. and Sim J. 2017 Progress in doping semiconductor nanowires during growth *Mater Sci Semicond Process.*, **62**, 135-155

[5] Cui Y, Duan X, Hu J and Lieber C M 2000 Doping and Electrical Transport in Silicon Nanowires *J. Phys. Chem. B* **104** 5213–6

[6] Storm K, Halvardsson F, Heurlin M, Lindgren D, Gustafsson A, Wu P M, Monemar B and Samuelson L 2012 Spatially resolved Hall effect measurement in a single semiconductor

nanowire. *Nat. Nanotechnol.* **7** 718–22

[7] Blömers C, Grap T, Lepsa M I, Moers J, Trellenkamp S, Grützmacher D, Lüth H and Schäpers T 2012 Hall effect measurements on InAs nanowires *Appl. Phys. Lett.* **101** 152106

[8] Perea D E, Hemesath E R, Schwalbach E J, Lensch-Falk J L, Voorhees P W and Lauhon L J 2009 Direct measurement of dopant distribution in an individual vapour-liquid-solid nanowire. *Nat. Nanotechnol.* **4** 315–9

[9] Liu C, Dai L, You L P, Xu W J and Qin G G 2008 Blueshift of electroluminescence from single n-InP nanowire/p-Si heterojunctions due to the Burstein-Moss effect. *Nanotechnology* **19** 465203

[10] Ketterer B, Uccelli E and Fontcuberta i Morral A 2012 Mobility and carrier density in p-type GaAs nanowires measured by transmission Raman spectroscopy *Nanoscale* **4** 1789

[11] Garnett E C, Tseng Y C, Khanal D R, Wu J, Bokor J and Yang P 2009 Dopant profiling and surface analysis of silicon nanowires using capacitance-voltage measurements *Nat. Nanotechnol.* **4** 311–4

[12] Wallentin J and Borgström M T 2011 Doping of semiconductor nanowires J. Mater. Res. 26 2142–56

[13] Chen Y, Pistol M-E and Anttu N 2016 Design for strong absorption in a nanowire array tandem solar cell *Sci. Rep.* **6** 32349

[14] Otnes G, Heurlin M, Zeng X and Borgström M T 2017 $In_{(x)}Ga_{(1-x)}P$ Nanowire Growth Dynamics Strongly Affected by Doping Using Diethylzinc *Nano Lett.* **17** 702–7

[15] Otnes G, Heurlin M, Graczyk M, Wallentin J, Jacobsson D, Berg A, Maximov I and Borgström M T 2016 Strategies to obtain pattern fidelity in nanowire growth from large-area surfaces patterned using nanoimprint lithography *Nano Res.* **9** 2852–61

[16] Jacobsson D, Persson J M, Kriegner D, Etzelstorfer T, Wallentin J, Wagner J B, Stangl J, Samuelson L, Deppert K and Borgström M T 2012 Particle-assisted $Ga_{(x)}In_{(1-x)}P$ nanowire growth for designed bandgap structures. *Nanotechnology* **23** 245601

[17] Wallentin J, Ek M, Wallenberg L R, Samuelson L and Borgström M T 2012 Electron trapping in InP nanowire FETs with stacking faults *Nano Lett.* **12** 151–5

[18] Heurlin M, Anttu N, Camus C, Samuelson L and Borgström M T 2015 In Situ Characterization of Nanowire Dimensions and Growth Dynamics by Optical Reflectance *Nano Lett.* **15** 3597–602

[19] Lindelöw F, Heurlin M, Otnes G, Dagytė V, Lindgren D, Hultin O, Storm K, Samuelson L and Borgström M 2016 Doping evaluation of InP nanowires for tandem junction solar cells *Nanotechnology* **27** 65706

[20] Hultin O, Otnes G, Borgström M T, Björk M, Samuelson L and Storm K 2016 Comparing Hall Effect and Field Effect Measurements on the Same Single Nanowire *Nano Lett.* **16** 205–11

[21] Lindgren D, Hultin O, Heurlin M, Storm K, Borgström M T, Samuelson L and Gustafsson A 2015 Study of carrier concentration in single InP nanowires by luminescence and Hall measurements. *Nanotechnology* **26** 45705

[22] Borgström M T, Norberg E, Wickert P, Nilsson H A, Trägårdh J, Dick K A, Statkute G, Ramvall P, Deppert K and Samuelson L 2008 Precursor evaluation for in situ InP nanowire doping. *Nanotechnology* **19** 445602

[23] Glas F, Harmand J-C and Patriarche G 2007 Why does wurtzite form in nanowires of III–V zinc blende semiconductors? Phys. Rev. Lett. 99 146101

[24] Yablonovitch E, Sandroff C J, Bhat R and Gmitter T 1987 Nearly ideal electronic properties of sulfide coated GaAs surfaces *Appl. Phys. Lett.* **51** 439–41

[25] Li J., Wang D., and Lapierre R. R., Advances in III-V semiconductor nanowires and nanodevices (Bentham), 2011, 59

[26] J. B. Mullin, A. Royle, B. W. Straunghan, P.J. Tufton and E.W. Williams, J. Crystal Growth 1972, **13/14**, 640

[27] Gutsche C, Regolin I, Blekker K, Lysov A, Prost W and Tegude F J 2009 Controllable p - type doping of GaAs nanowires during vapor-liquid-solid growth *J. Appl. Phys.* **105** 0–5

[28] Levinshtein M, Rumyantsev S and Shur M 1996 Handbook Series on Semiconductor Parameters vol 2 (Singapore: World Scientific)